




The Impact of Warm Core Rings on Middle Atlantic Bight Shelf Temperature and Shelf Break Velocity

Jacob Forsyth^{1,2} , Glen Gawarkiewicz¹ , and Magdalena Andres¹ 

¹Department of Physical Oceanography, Woods Hole Oceanographic Institution, Woods Hole, MA, USA, ²Department of Earth, Atmospheric, and Planetary Sciences, Massachusetts Institute of Technology, Cambridge, MA, USA

Key Points:

- Warm Core Rings with higher azimuthal velocities lead to larger anomalies of shelf velocities
- There is a strong area of divergence of cross-shelf velocities near the trailing edge of rings with inferred upwelling rates of 10–100 m/day
- Rings tend to cool a stratified shelf during warmer months and warm a mixed shelf in cooler months

Correspondence to:

J. Forsyth,
jakesforsyth@gmail.com

Citation:

Forsyth, J., Gawarkiewicz, G., & Andres, M. (2022). The impact of Warm Core Rings on Middle Atlantic Bight shelf temperature and shelf break velocity. *Journal of Geophysical Research: Oceans*, 127, e2021JC017759. <https://doi.org/10.1029/2021JC017759>

Received 8 JUL 2021
Accepted 24 FEB 2022

Abstract Warm Core Rings (WCRs) are known to disrupt the shelf flow as well as drive strong heat transport onto the Middle Atlantic Bight shelf. We examine 27 rings sampled by the container ship *Oleander*, 16 rings which have in-situ velocity data and 11 rings identified from satellite sea surface height but with in-situ temperature data, to study the variability in rings' impact on shelf break velocities and on the temperature of the adjacent shelf. WCRs that have higher rotational velocities and are closer to the shelf are found to exert greater influence on the along-shelf velocities, with the fastest and closest rings reversing the direction of flow at the shelf break. As rings approach the study site, the Shelfbreak Jet is faster than when the rings are about to exit the study site, likely due to first steepening then flattening of the isopycnals at the Shelfbreak Front. Rings also have lasting impacts on the shelf temperature: rings with faster rotational velocities cool the shelf and rings with slower rotational velocities warm the shelf. The evolution of temperature on the shelf as a ring passes is strongly tied to the season. During warmer seasons, when temperature stratification on the shelf is strong, a ring cools the shelf; during periods of weak thermal stratification, rings tend to warm the shelf. Rings which cool the shelf are additionally associated with increased upwelling as they pass the study site.

Plain Language Summary Warm Core Rings are large rotating masses of Gulf Stream water that have been isolated from the Gulf Stream and move through the Slope Sea next to the shelf. We identify and study 16 rings from ship board observations off the coast of New Jersey, and additionally study 11 more rings using a combination of limited ship observations and satellite data. Typical velocities at the shelf break in this region are to the southwest. Rings which rotate more quickly tend to disrupt the normal velocities over the shelf and shelf break and can even reverse these currents. As a ring approaches the study site the southwest velocities over the shelf break are enhanced, and when a ring is exiting the study site the southwest velocities at the shelf break are reduced. Rings exert a lasting influence on the temperature on the shelf. During warmer seasons, rings tend to cool the shelf, while in cooler seasons rings tend to warm the shelf.

1. Introduction

Warm Core Rings (WCRs) form from large meanders of the Gulf Stream that are pinched off, leaving an anti-cyclonic eddy of warm salty water north of the Gulf Stream. These rings can abut the Middle Atlantic Bight (MAB) shelf as they move westward through the Slope Sea until they are reabsorbed into the Gulf Stream. Disruptions to mean shelf break currents as well as large shelf temperature anomalies have been attributed to adjacent rings (e.g., Beardsley et al., 1985; Forsyth et al., 2020; Gawarkiewicz et al., 2019). Observations have shown that more rings have been formed annually since 2000, leading to the possibility that there are more frequent disruptions to the shelf system (Gangopadhyay et al., 2019). With this increase in the number of ring formations per year, understanding how rings are able to impact the shelf is increasingly important.

Early studies of WCRs combined limited in-situ observations with satellite thermal imaging to study the properties of the rings and their interactions with the shelf (e.g., Bisagni, 1983; Churchill et al., 1986; Joyce, 1984; Morgan & Bishop, 1977). These studies quantified dynamical properties of the rings, and estimated cross-shelf fluxes associated with warm streamers which cross onto the shelf even as the ring core remains over the slope. Estimates of the ring-driven cross-shelf heat flux suggest that they play a key role in the yearly heat budget for the shelf (Morgan & Bishop, 1977). Individual shelf streamers were also observed to carry a significant fraction of the annual slope water transport to the shelf as estimated from salinity (Churchill et al., 1986). The cross-shelf water mass exchange is modified by both warm streamers moving onto the shelf, and also cold streamers pulled

© 2022. The Authors.

This is an open access article under the terms of the [Creative Commons Attribution License](https://creativecommons.org/licenses/by/4.0/), which permits use, distribution and reproduction in any medium, provided the original work is properly cited.

off of the shelf by WCRs (Cenedese et al., 2013; Wei et al., 2008). Cold streamers have been estimated to transport approximately 1 Sv offshore, depositing the water between the ring and the Gulf Stream (Joyce et al., 1992).

Observations on the shelf have shown that WCRs impact the shelf circulation and the Shelfbreak Jet (e.g., Beard-sley et al., 1985; Gawarkiewicz et al., 2001; Pickart et al., 1999). Pickart et al. (1999) found that a WCR forced a large meander in the Shelfbreak Jet pushing the jet onshore, while Gawarkiewicz et al. (2001) observed that the Shelfbreak Jet was accelerated/slowed on the leading/trailing edge of the ring. Recent modeling studies describe various processes which enhance cross-shelf transport and disruptions of the shelf circulation (Chen et al., 2014; Zhang & Gawarkiewicz, 2015). In particular, Zhang and Gawarkiewicz (2015) described one process by which ring water intrudes directly onto the shelf through a “Pinocchio's nose” intrusion that resulted from vorticity variations within a warm limb of the ring.

One of the main limitations of many previous WCR studies is that they are typically restricted to “case studies” that detail the dynamics of only one or two rings. In contrast, underway shipboard observations from the CMV *Oleander* give repeat transects since 1992 between New Jersey and Bermuda, allowing for the study of many rings sampled from the same observational platform. The CMV *Oleander* is equipped with instrumentation to measure profiles of water velocity and temperature, as well as near-surface temperature and salinity, such that both dynamical and hydrographic properties of the ring and shelf system can be quantified. Observing many rings allows us to describe how rings can differ from each other, and how rings with varying properties are able to impact the shelf and shelf break.

This study builds on the results of Forsyth et al. (2020), which used the CMV *Oleander* data to characterize the mean Shelfbreak Jet in both Eulerian and stream coordinate frames. In that study, the Jet was found to be ephemeral, present only in 60% of the velocity sections. In many cases when the Jet could not be identified in a velocity section, the presence of a WCR was detected, so this followup study focuses on the rings and their impact.

We describe the data from the CMV *Oleander* and the method used to identify the transects that sample through a WCR in Section 2.1. Additionally, Section 2.2 details data derived from satellites including eddy tracking of the WCRs. The impact WCRs have on shelf circulation and parametric dependencies between different WCRs is discussed in Section 3.1. We examine the lasting impact of rings on shelf temperature by comparing the conditions before and after a ring passes in Section 3.2. Section 4 summarizes our findings.

2. Methodology

WCRs regularly cross the Oleander Line, moving slowly along the continental slope, and many of these happen to be sampled on the Oleander's regular transects. In order to fully capitalize on the various Oleander data sets, and to characterize rings with as many in situ measurements as possible, multiple data sources are used to identify rings that cross the Oleander Line. In total, 27 rings are examined here. Of these, 16 are identified directly, using the in situ velocity profiles from the Oleander's shipboard acoustic Doppler current profiler (ADCP). An additional 11 are identified using remote sensing, relying on the Chelton data set which identifies and tracks WCRs using mapped sea surface height (SSH) (Chelton et al., 2011). Of the 16 rings identified with the Oleander velocity profiles, 12 have in situ temperature profiles that were measured both before and after a given ring passed. All of the 11 rings that were identified using the Chelton data have temperature profiles bracketing the ring's passage across the Oleander Line. Hence analysis of the impact of rings events on temperature relies on 23 rings, whereas analysis of the impact on shelf and shelf break velocity uses only 16 rings.

2.1. CMV *Oleander*

The CMV *Oleander* has recorded upper-ocean velocity profiles using ADCPs since 1992 on its weekly round trips between Port Elizabeth, New Jersey and Bermuda (Figure 1). In addition to the ADCP data, temperature profiles from expendable bathythermographs (XBTs) have been measured across the transect approximately once a month since 1977. In 2000 a thermosalinograph (TSG) began measuring the near-surface temperature and salinity. The data acquisition, quality control, and gridding methodology for the ADCP and XBT data are described previously (Flagg et al., 1998; Forsyth et al., 2015, 2020). Minor changes to the methodology implemented to better study individual rings are described here.

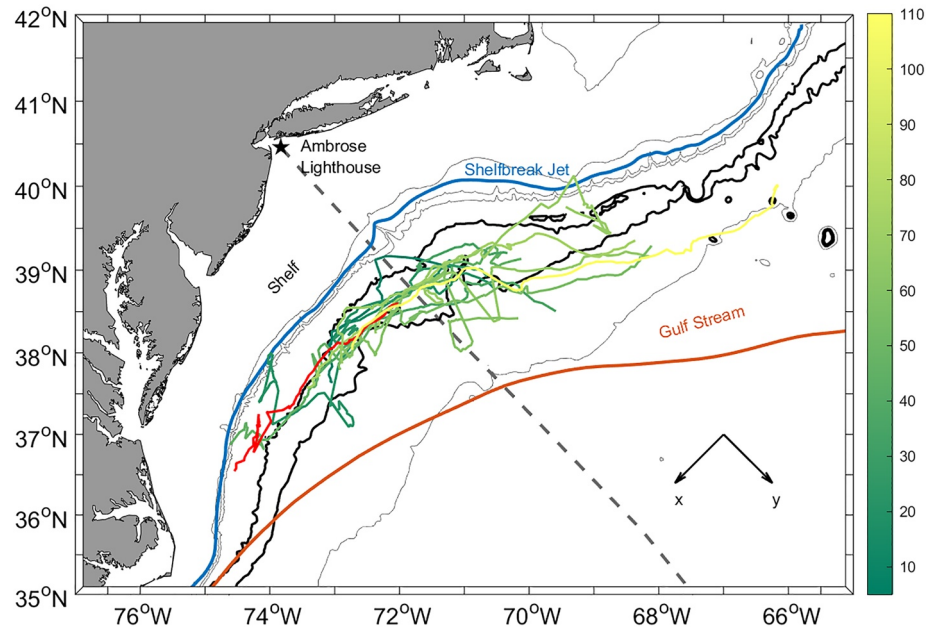


Figure 1. Eddy tracks of 14 Warm Core Rings (of 16 total) that have acoustic Doppler current profiler data and can be identified using the Chelton eddy tracks. Colors indicate the age of the ring in days when it crosses the CMV *Oleander* Line (Chelton et al., 2011). One ring track does not cross the Oleander Line in the Chelton Tracks and is plotted in red. The gray dashed line shows the Oleander Line, the orange solid line is the mean position of the Gulf Stream (as defined by the 25 cm sea surface height contour), and the blue line is the approximate position of the Shelfbreak Jet which is located over the shelf break. The axes are shown in the bottom right. Contours of the 100, 500, and 4,000-m isobaths are plotted in gray, with the 2,400 and 2,900-m isobaths plotted in black. The shelf region is onshore of the shallowest (100 m) contour. The Slope Sea occupies the area between the shelf and the Gulf Stream.

For the ADCP data, we modify the gridding utilized in previous research to retain as high a resolution as possible (Forsyth et al., 2020). Based on the characteristics of individual rings, the horizontal grid scale chosen here is 3 km, and the vertical grid is 4 m on the shelf and 8 m in deeper regions. Data that were acquired with coarser vertical resolution (rings after the year 2005) are linearly interpolated to match the vertical resolutions given above. Due to different data acquisition settings over the shelf and the deeper ocean, the shallowest bin of data is centered at 8 and 16 m for the shelf waters and the deeper ocean respectively. The data are rotated in the along-shelf (x -axis, southwest) and cross-shelf (y -axis, southeast) direction (axis in Figure 1).

XBT data are gridded on a 30 km horizontal by 10 m vertical grid, with the top vertical bin between 0 and 10 m. This is coarser than the grid used in our previous analyses with these data (Forsyth et al., 2015), but is more representative of the resolution of the raw data during the time period when most rings were observed in the ADCP data set. We do not use any data filling techniques for the XBT sections in order to preserve the signals from individual events (i.e., we do not relax to a monthly climatology when XBT profiles are missing). The temperature impact of rings on the shelf is quantified using temperature anomalies. To calculate the shelf temperature anomalies, we remove the seasonal signal from the gridded data. This is done by calculating average temperature sections for each month using XBT data from 1977 to 2018, and then subtracting the average monthly temperature section from the gridded data in the corresponding month. Finally, we calculate a spatially averaged shelf temperature anomaly for the area between the 40 and 100 m isobaths (90 km horizontal range with our spatial grid).

WCRs tend to move across the Oleander Line from the northeast to southwest and velocities measured on the fixed Oleander Line evolve as a ring moves by. As the leading edge of the ring approaches the Oleander Line, the anti-cyclonic velocity signatures are observed to be onshore. Over time, when the CMV *Oleander* is sampling the middle of the ring, the largest velocities are in the along-shelf direction with Northeastward velocities closer to the shelf and Southwestward velocities further offshore. When the trailing edge of the ring is on the Oleander Line, the velocities measured are in the offshore direction.

Based on how the CMV *Oleander* samples a ring, we develop a methodology to identify velocity sections with WCR influence. A section with a ring is defined by having two local maxima in the depth-averaged along-shelf velocity greater than 10.15 m s^{-1} , a threshold based on previous work (Forsyth et al., 2020). The onshore local maximum must have velocity in the northeast direction, with the velocity maximum located further offshore directed toward the southwest, thereby identifying an anti-cyclonic velocity signature. Lastly, we include sections without anti-cyclonic velocity signatures if they are consistent with the velocities anticipated on the leading and trailing edge of the ring, and occur before and after sections with anti-cyclonic velocity respectively. We identify 16 rings between 1997 and 2008 that are sampled by 5 or more ADCP sections. These rings take an average of 30 days to pass over the Oleander Line, with around 80% of the transects sampling through the broad “middle” of the ring and the rest sampling a leading or trailing edge.

After the ADCP sections with ring signatures are selected, we compile all available TSG and XBT data that occur before, during, and after each individual ring. TSG data are only available for 8 rings, while XBT data are partially available for each ring. 12 rings have XBT data within one month before and also within one month after the ring has passed through the Oleander Line, while 13 rings have XBT data that samples the ring directly.

2.2. Satellite Data

Satellite sea surface temperature (SST) and SSH data have been used in many ring studies. As the CMV *Oleander* provides only a 2-d (vertical section) perspective of the rings, satellite data provide valuable spatial context for these rings. We use National Oceanographic and Atmospheric Administration (NOAA) Optimum Interpolation (OI) $\frac{1}{4}^\circ$ daily SST (AVHRR-only; Reynolds et al. (2007)). For SSH data and SSH-derived geostrophic velocities, we use daily mapped absolute dynamic topography at $\frac{1}{4}^\circ$ resolution, available through E.U. Copernicus Marine Environmental Monitoring Service. Lastly, mapped ocean chlorophyll data from satellites are used from the Ocean Biology Processing Group (OBPG) Sea-viewing Wide Field-of-view Sensor (SeaWiFS) which reports data at a 4 km resolution.

Additionally, we use eddy tracks from Chelton et al. (2011) to examine the path taken by each ring that we observe crossing the Oleander Line. Two of the 16 rings cannot be found in the eddy tracks as they do not last for 28 days as required to be included in the Chelton eddy tracks. For the remaining 14 rings, for which we do have the Chelton tracks, we calculate the age of the ring, or how long each ring has existed before it crosses the Oleander Line (colored lines in Figure 1). If a ring crosses the Oleander Line multiple times, we calculate the age of the ring during the crossing when the ring is closest to the shelf break. The age of the ring ranges from 6 to 109 days, with one ring never crossing the Oleander Line (as represented in the Chelton tracks). The ring which does not cross the Oleander Line was formed just south of the Oleander Line and stayed within the region long enough that there are over five sections of ADCP data through the ring despite the center never crossing over the Oleander Line. All but one of the rings intersect the Oleander Line between the 2400 and 2900-m isobaths. The rings are tightly bounded by these isobaths, indicating strong topographic trapping.

We compute from the ADCP measurements the maximum speed in each ring section as a proxy for azimuthal velocity, assuming the predominant motion within the rings is azimuthal and not radial. We then compare this with azimuthal geostrophic velocities derived from the SSH fields. There is an average difference between the azimuthal velocity derived from SSH and the azimuthal velocity calculated from the ADCP data of 0.5 m s^{-1} (Figure 2). Throughout individual sections, these two quantities are correlated linearly with larger differences at higher speeds/velocities. While these quantities are not measuring the same properties, this indicates that in-situ velocities are needed to accurately reflect the flows within rings. Comparisons between CMV *Oleander* ADCP data and SSH fields have shown good agreement in regions of low variance, however, in regions with higher variance, that is, energetic rings, the consistency between the two measurements is reduced (Worst et al., 2014).

There are rings in the Chelton tracks that do not have reliable ADCP data but do have XBT sections. To include as many rings as possible in the analysis of ring influence on shelf temperatures, an additional 11 rings are included. These 11 rings are identified from the Chelton tracks and have XBT data available within one month before and also within one month after a ring has passed the CMV *Oleander* line. We approximate the velocity of these rings by inferring the velocities that would be measured by the ADCP by using the linear fit between the SSH-derived

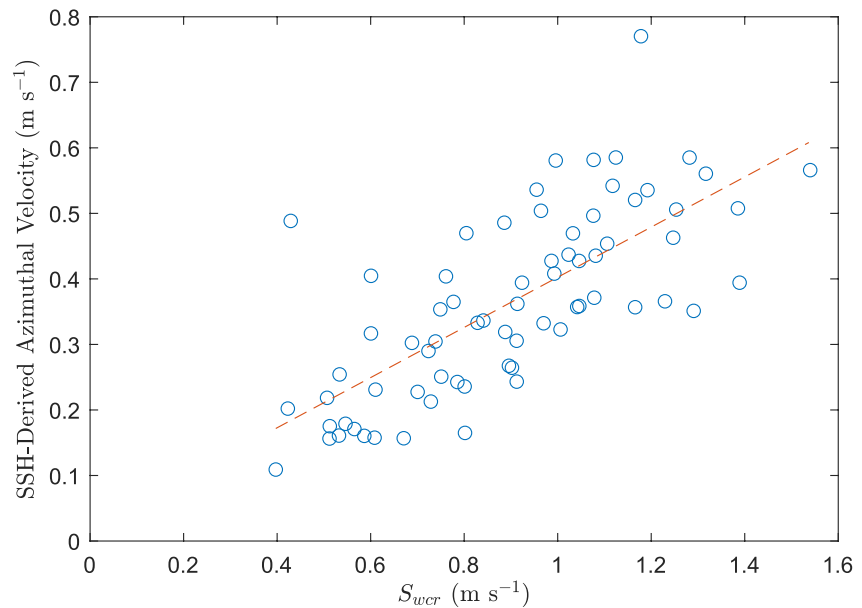


Figure 2. Sea surface height (SSH) derived azimuthal velocity from the Chelton tracks plotted against acoustic Doppler current profiler (ADCP) calculated ring speed in each ring section (S_{wcr}) in blue circles. The best linear fit line is plotted in the dashed red line. The comparison here is from 14 rings which are identified in both the ADCP and Chelton tracks. 71 sections have the required data coverage for this calculation.

velocities and the ring speed (Figure 2). In total, this gives 23 rings with XBT data before and after the ring, and a total of 16 rings with XBT sections that sample directly within the ring.

3. Results

3.1. Warm Core Ring Impact on Shelf Break Velocities

In total, for the 16 WCRs with ADCP data, we have 151 velocity sections within the WCRs. Of the 151 velocity sections, 122 measure the center of the rings and are used for the calculation of ring properties unless we specify the study of the leading and trailing edge (not all rings have measurements through the leading or trailing edges). From these 122 velocity sections we create an Eulerian mean WCR section (Figure 3). Flow is primarily in the along-shelf direction, with weak onshore velocities throughout the slope and shelf. This net onshore flow over the slope is likely an artifact resulting from having more sections that sampled the leading edge of the ring where flow would be expected to be in the onshore direction. The northeastward velocities of the mean Eulerian WCR section show enhanced flow subsurface with maximum velocities at around 80 m depth. The mean velocity field represented by this Eulerian average is of limited use as the different rings included in the study show large variations in their velocity structures as exhibited by the standard deviations. Additionally, our sub-sample of 16 rings (a small fraction of the total number of rings that crossed the Oleander Line during this time) may not accurately represent the distribution of velocities that would be observed with a larger sample of rings.

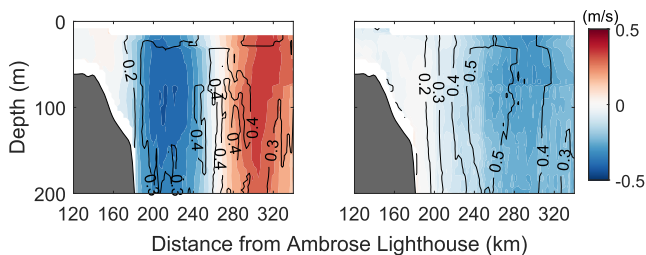


Figure 3. Eulerian mean along-shelf velocity (left column) and cross-shelf velocity (right column) from 122 sections sampling the “middle” of the Warm Core Rings. Standard deviations (m/s) are plotted in the black contour lines.

Focusing on the velocity structure over the shelf onshore of the WCRs, the 122-section Eulerian mean shows a Shelfbreak Jet during time periods when WCRs are in the Slope Sea (Figure 4). In comparison to an Eulerian mean calculated for all 1362 CMV *Oleander* ADCP sections (Forsyth et al., 2020), the Eulerian mean Shelfbreak Jet during WCRs is shifted onshore, is narrower, and has weaker transport, but a similar maximum velocity. This is consistent with the hypothesis from (Forsyth et al., 2020) that WCRs can shift the Shelfbreak Jet onshore and is consistent with past research on rings (Pickart et al., 1999). Overall, we still find an Eulerian mean Shelfbreak

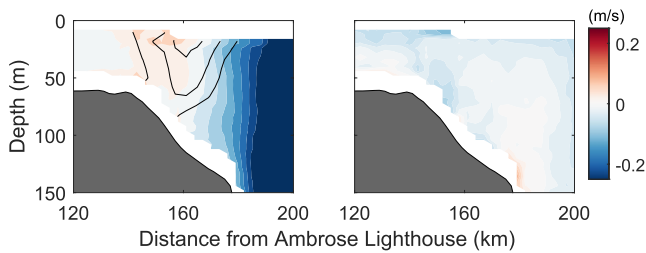


Figure 4. Eulerian mean along-shelf velocity (left column) and cross-shelf velocity (right column) from 122 sections sampling the “middle” of the Warm Core Rings. The color bar is half the range as Figure 3. Black contours are the 0.06, 0.08, and 0.10 m s^{-1} isotachs calculated from the Eulerian mean along-shelf velocity (Forsyth et al., 2020).

Jet during WCRs indicating that not all WCRs reverse the flow at the Shelfbreak Jet as found during specific individual ring events (Beardsley et al., 1985; Chen et al., 2014; Zhang & Gawarkiewicz, 2015). In order to understand how rings impact the shelf flows, we need to examine individual rings and consider the ring proximity to the Oleander Line.

To examine individual rings and quantify their impact on the shelf, rather than focus on composite averaged ring properties, we calculate several ring and shelf parameters and examine how they co-vary. We calculate the ring speed, S_{wcr} , by finding the maximum northeast and southwest depth-averaged velocity (top 100 m) in each ring section and then average the absolute value of these two depth-averaged velocities. To calculate the ring radius, r_{wcr} , we identify the e-folding isotach from the ring speed and calculate the distance between this isotach on either side of the ring and divide in half. Using this isotach, we also calculate d_{sb} , the distance of the onshore edge of the ring to the shelf break

(the choice of isotach to mark the edge of the ring does not significantly impact the relationships discussed below). The ring speeds of our 16 rings range from 0.22 to 0.88 m s^{-1} with the ring radii ranging from 50 to 85 km radius.

In order to quantify the impact of rings on the shelf velocity structure, we calculate the velocity at the mean Eulerian position of the Shelfbreak Jet by averaging the along-shelf velocities in a 40 km horizontal by 60 m vertical box based on the e-folding scale of the Shelfbreak Jet centered over the 115-m isobath (methodology described in Forsyth et al. (2020)). We linearly regress the velocity at the shelf break onto S_{wcr} and d_{sb} , and find significant linear relationships with the two variables ($p < 0.01$). This relationship indicates that the faster and closer a ring is to the shelf break, the more negative (northeast) the along-shelf flow is. Cases when the ring is slow and far from the shelf break tend to have a shelf break velocity that is more typical of mean shelf break conditions, or southwest flow (Forsyth et al., 2020). It is important to note that S_{wcr} and d_{sb} are not correlated with one another (despite each one's correlation with flow at the shelf break). Repeating the regression calculations with the shelf's maximum along-shelf velocity (rather than velocity at the shelf break) results in similar relationships, where faster and closer rings reduce the southwest along-shelf flow on the shelf.

Rings impact on the velocity field at the Oleander Line evolves as the ring crosses the transect. To examine a ring's impact over time on the velocity field, we calculate composite (Eulerian) averages for the sections influenced by the rings' leading and trailing edges, using observations from the 16 rings with ADCP measurements (Figure 6). The leading edge average is calculated using the first transect where ring influences are observed from each ring, whereas the lagging edge is calculated from the last velocity transect where ring influences can be seen (designation of when we determine ring influences occur described in Section 2). The composite averages suggest that at the leading edge of the ring, cross-shelf velocities are all onshore within the ring and over the shelf (Figure 6b). In the Eulerian means using the final section from each ring, the cross-shelf velocity shows a strong divergence at the location of the maximum equatorward flows in the along-shelf velocity which is the Shelfbreak Jet (Figures 6c and 6d), at 175 km). This divergence of the cross-shelf velocities can be seen, not only in the composite, but also in each individual ring's last transect, with onshore velocities at the shelf break, and offshore velocities in the ring over the slope. The location of the divergence point is at the same location as the maximum equatorward flows, and is likely associated with the offshore deflection of the Shelfbreak Jet.

Along-shelf velocities within the Shelfbreak Jet are strongest on the leading edge of the ring, with the maximum Eulerian mean velocities reaching 0.2 m s^{-1} in the surface layers (Figure 6a). The Shelfbreak Jet at the leading edge of the ring is faster than the total Eulerian mean Shelfbreak Jet velocities, though with similar width and depth scales of 50 km and 80 m respectively (Forsyth et al., 2020). As the ring passes, we see the Eulerian mean Shelfbreak Jet velocities decrease and become narrower. In the Eulerian mean last section of the WCRs, the equatorward Shelfbreak Jet is surface trapped, with weaker velocities (Figure 6d). The strengthening and weakening of the Shelfbreak Jet as the ring approaches and then moves away is consistent with past research (Gawarkiewicz et al., 2001; Pickart et al., 1999). In Gawarkiewicz et al. (2001), the strengthening of the Shelfbreak Jet on the leading edge of the ring was attributed to the steepening of the isopycnals in the Shelfbreak Front while the weaker jet on the trailing edge of the ring was attributed to the flattening of the isopycnals in the Shelfbreak Front. This velocity result also holds true without using composite averages. On average, the equatorward shelf break velocities are 0.05 m s^{-1} faster on the leading edge compared to the trailing edge.

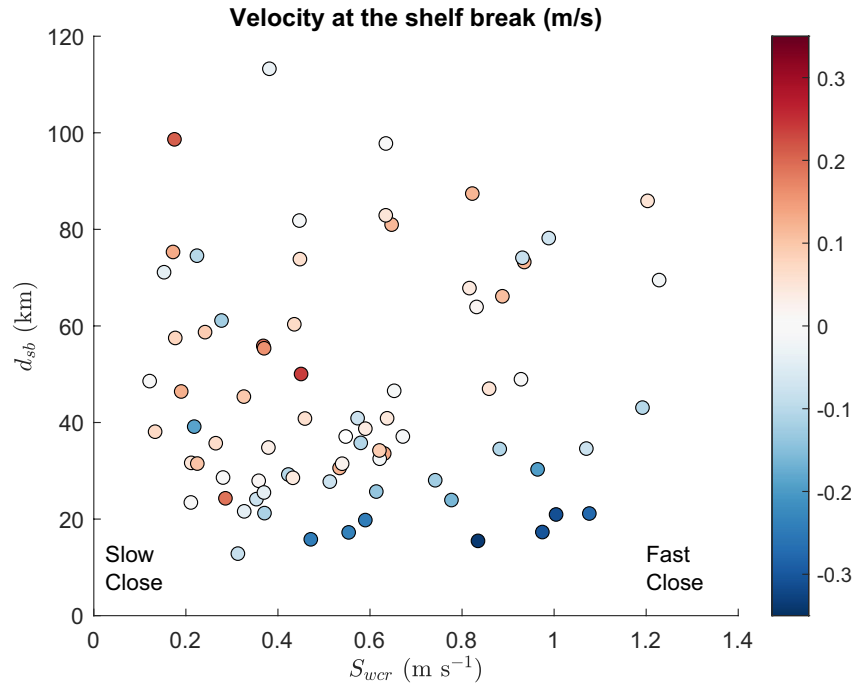


Figure 5. The velocity at the shelf break plotted in colors, as a function of the ring speed (S_{wcr} , x-axis) and distance from the shelf break (d_{sb} , y-axis). A linear regression model shows both independent variables have significant relationships to the velocity at the shelf break ($p < 0.01$).

A composite average from the sections that sample the middle of the ring, excluding the leading and trailing edges, has maximum equatorward flows at 0.05 m s^{-1} which are typical for mid-shelf flows on the MAB and not the Shelfbreak Jet (Lentz, 2008). The reversal of the flows at the shelf break (as found in Figure 5) only occurs when the Oleander Line samples through the center of the ring and not at the leading or trailing edge. A ring takes an average of 30 days to pass over the Oleander Line, leading to around 80% of the transects in rings to be through the middle. The enhancement of the Shelfbreak Jet can only be seen over one or two transects per ring, suggesting this only lasts on the order of a week, while the reversal of flow due to a ring can last on the order of a month.

We estimate the upwelling at the trailing edge of the ring in this frontal region between shelf and ring water. We assume the divergence at the surface is equivalent to that at our surface-most bin (16 m) and also assume that the vertical velocities are zero at the surface ($z = 0$). Given those assumptions, we can calculate the upwelling from the rearranged continuity equation

$$w_{up} = - \left(\frac{\partial u}{\partial x} + \frac{\partial v}{\partial y} \right) \cdot dz. \quad (1)$$

We use $\frac{\partial u}{\partial x}$ from a previous study of WCRs with a value of $-1 \cdot 10^{-5} \text{ s}^{-1}$ (Gawarkiewicz et al., 2001). Estimates of $\frac{\partial u}{\partial x}$ from calculations of ∂t and a ring translation speed are unreliable as the time between transects of good data varies from a few days to weeks. For the 13 rings with sufficient data in the last section of the ring, we calculate $\frac{\partial v}{\partial y}$ at each depth layer above 50 m and find the location of the maximum divergence. Next we take the depth averaged cross-shelf velocity divergence and use that value in Equation 1. The value for dz used is 34 m which is the difference between the shallowest bin used (16 m for the ADCP data gathered over the slope) and the deepest bin used (50 m).

This results in a range of w_{up} values between 9 and 100 m day^{-1} , and the average of the 13 rings w_{up} as 63 m day^{-1} . Our values are generally larger than a previous calculation on the trailing edge of a WCR of approximately 20 m day^{-1} (Gawarkiewicz et al., 2001). However, the ring with the weakest w_{up} , 9 m day^{-1} , is consistent with past research of upwelling in the Shelfbreak Front calculated from ADCPs, and calculated in a dye release experiment (Barth et al., 1998; Houghton & Visbeck, 1998). This specific ring has the weakest ring speed, and the Shelfbreak Jet can be observed in every individual transect during the ring. As this ring didn't impact the Shelfbreak Jet, we

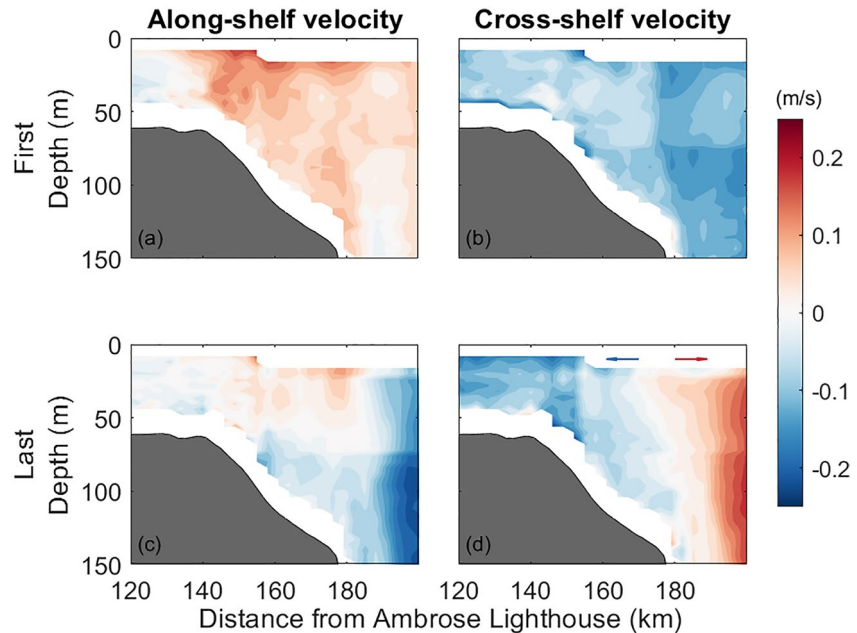


Figure 6. Composite averages of along-shelf velocity (left column) and cross-shelf velocity (right column) during the first ring section of each ring (top row), and during the last ring section of each ring (bottom row). In the cross-shelf velocity during the last ring section (d), we label the direction of the flow indicating divergence.

believe our estimate of 9 m day^{-1} to represent a time period where the shelf is not affected by the ring and thus the consistency with past research verifies that our estimates of upwelling are accurate to first order. Overall, we see a large increase in upwelling as the ring passes.

Enhanced upwelling is typically associated with increased nutrients and chlorophyll, and past research has found increased chlorophyll and dense marine mammal sightings at the trailing frontal region of rings (J. P. Ryan et al., 1999; Griffin, 1999). Satellite chlorophyll measurements do not show significant increases in chlorophyll after a ring passes. However, peak chlorophyll values at the Shelfbreak Front are often subsurface, and enhanced chlorophyll values have been observed after intrusions of Gulf Stream water onto the shelf (Oliver et al., 2021). Satellite chlorophyll measurements could miss some of the impact that WCRs have on the shelf/slope chlorophyll. Surface chlorophyll anomalies within rings have also been shown to have inconsistent responses to the rings (Ning et al., 2021).

We do note that chlorophyll can act as a tracer for shelf water given the correct initial conditions. A ring crossing the Oleander Line in April 1999 during a bloom indicates offshore advection by the ring, moving water from the shelf onto the slope. As the ring moves toward the Oleander Line (distinguished by the circular SSH contours in Figure 7), it has extremely low chlorophyll relative to the slope and shelf waters (Figure 7a). When the ring reaches the Oleander line, the chlorophyll increases inside the ring, with increases starting on the trailing edge (Figure 7b). As the chlorophyll bloom ends in the Slope Sea, the only enhanced values of chlorophyll remaining in the Slope Sea are found inside the ring (Figure 7d). This interaction in early spring is seen in two additional rings analyzed within this study (May 2000 and April 2004). While surface chlorophyll is insignificantly changed relative to the upwelling values at the trailing edge of a ring, a ring's interaction with shelf water leads to streamers that can draw the surface chlorophyll out into the Slope Sea impacting the ecology of the slope.

3.2. Warm Core Ring Impact on Shelf Temperature

In order to understand the lasting impact that rings have on the shelf temperature, we focus on the 23 rings (identified from both satellites and ADCP data) that have XBT data before and after a ring passage. We calculate ΔT_s , which is the difference between the spatially averaged shelf temperature anomaly after and before the ring crosses the Oleander Line (the spatially averaged shelf temperature anomaly is calculated as described in Section 2.1). Of the 23 rings with XBT data before and after the ring, 9 of the rings show shelf cooling (negative ΔT_s) while 14 rings show a shelf warming (positive ΔT_s , Figure 8). The XBT sections are taken at different time intervals

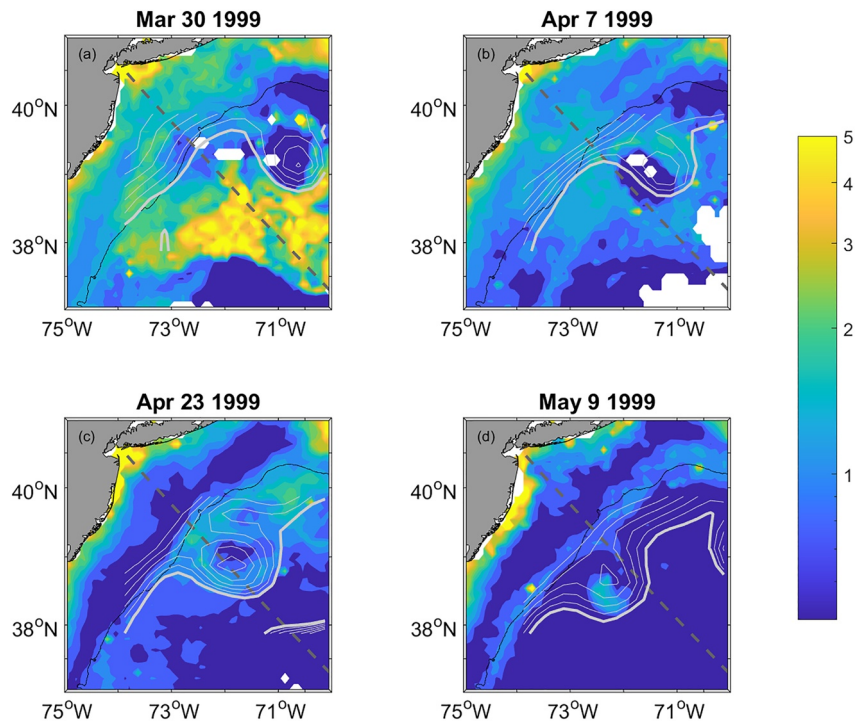


Figure 7. Satellite chlorophyll-a measurements during a ring analyzed in this study in colored contours. Light gray contours mark sea surface height contours at 2 cm intervals, with the thicker light gray contour representing the -25 cm SSH. The black line is the 100-m isobath. The gray dashed line shows the Oleander Line.

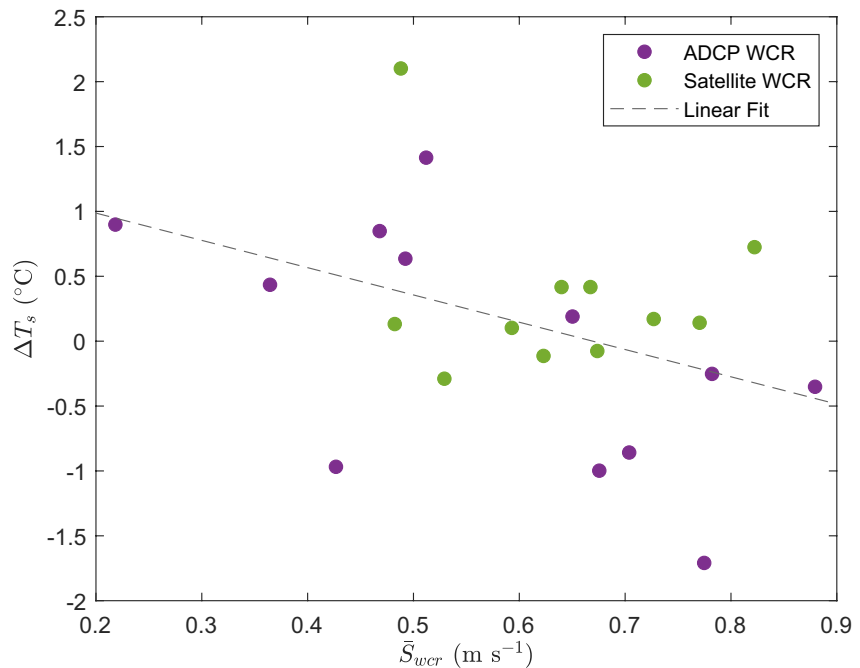


Figure 8. Change in spatially averaged shelf temperature anomalies before and after a ring (ΔT_s) plotted against the average speed of each ring (\bar{S}_{wcr}). Rings with speed calculated from the direct acoustic Doppler current profiler (ADCP) measurements in purple, and rings with speed calculated from sea surface height-derived velocity and then fit to approximate ADCP speed in green. The two variables with the 12 rings using expendable bathythermographs and ADCP measurements are significantly anti-correlated at the 95% confidence interval ($r = -0.58$ and $p < 0.05$), while the total 23 rings are less correlated ($r = -0.41$ and $p < 0.06$). Gray dashed line shows the linear fit of the total 23 rings.

after the ring has passed, however, there is no correlation between ΔT_s and the timing of the final XBT sections after the ring has passed. This suggests that other factors are more important in determining the impact on the shelf temperature than time since a ring has passed. We also calculate the change in SST anomaly on the shelf where we remove the seasonal cycle in the data. We then calculate the change in shelf temperature anomaly over the same horizontal area for which we have XBT profiles, as well as using the same dates as when the XBTs were taken. There is no significant correlation between ΔT_s and the change in SST anomaly during rings at the 95% confidence interval. This lack of correlation suggests there is a difference in how rings impact the surface temperature and the depth averaged temperature. The change in temperature is likely not uniform through each depth layer.

In order to compare a singular temperature section to properties derived from multiple velocity sections, we average properties found in each section to obtain the average property for each particular ring (between 5 and 19 sections for each ring). Properties that are averaged over multiple sections will be denoted with a bar, \bar{S}_{wcr} is the average S_{wcr} as calculated in Section 3.1.

\bar{S}_{wcr} and ΔT_s are significantly anti-correlated at the 95% confidence interval when only considering the 12 rings with XBT data that are identified from the ADCP data (Figure 8). This relationship is weaker when including all 23 rings with XBT data (significant at 94% confidence interval), though the speeds calculated from altimetry are subject to larger uncertainty (due to spatial resolution, data mapping, and the fit to estimate total velocity). Faster rings tend to have a cooling relationship with the shelf, while slower rings have a warming relationship. To understand why this is so, we examine the structure of velocities within the core of the 16 rings with ADCP data, as well as the seasonality of the rings.

As seen in the Eulerian mean velocity section of the rings (Figure 3), a subsurface velocity maximum exists in the core of the onshore side of the ring. We identify the depth at which the velocity maximum occurs in both the northeast and southwest velocity maximums for each section of every ring, and then average the depths found in each section to get, \bar{z}_{max} , the average depth of the velocity maximum. The difference between the depth of velocity maximums in the onshore and offshore sides of the ring are highly correlated and not significantly different from each other. We find that only two rings have \bar{z}_{max} above 50 m, and half of the 16 rings studied have \bar{z}_{max} below 80 m. Correlating \bar{z}_{max} to ΔT_s , the relationship is not significant ($r = 0.44$ and $p > 0.15$), however, it becomes significant if we remove the ring with the smallest \bar{S}_{wcr} ($r = 0.62$ and $p < 0.05$). As mentioned above, the weakest ring had no impact on the Shelfbreak Jet, and additionally is one of the rings that cannot be tracked through the Chelton analysis. w_{up} for this ring was also consistent with studies that estimated upwelling when no rings were present. Thus, removing this atypical ring to study the depth of the maximum velocity seems appropriate.

The correlation suggests that rings with deeper \bar{z}_{max} have ΔT_s that is positive, while shallower \bar{z}_{max} rings tend to cool the shelf. The reasoning for the relationship between the depth of the rings' maximum velocity and the changing shelf temperature is unclear at present. However, the finding that rings have primarily sub-surface intensified velocities is important to report so future model-focused studies can further investigate this velocity structure.

Rings tend to have the largest \bar{S}_{wcr} during the summer months, in June and July, with high speeds as well in spring (Figure 9). Summer is also the time period when rings are most commonly observed (Gangopadhyay et al., 2020). Unfortunately, we do not observe many rings in January-March as data quality in the winter months from the CMV *Oleander* ADCPs are the least reliable (due to bubble noise). As such, no WCRs during these months had the prerequisite five sections of reliable ADCP data through them, though satellite tracking identifies two rings in February-March. The temperature structure of the rings observed has a strong seasonal signal. We look at the temperature difference between the surface and 100 m depth in each ring with XBT data during the ring (16 rings), defined as δT_{wcr} . δT_{wcr} is largest within the summer months, reaching up to 14°C, and weakest during April and May. During April and May, the largest δT_{wcr} is only 2°C, with three rings having a δT_{wcr} less than 0.5°C. δT_{wcr} is correlated with ΔT_s at the 90% confidence level ($r = -0.53$ and $p = 0.09$), however, this likely due to the seasonal differences on the shelf as discussed next.

During June and July, the MAB Cold Pool is well established (Forsyth et al., 2015). We calculate the surface-to-bottom temperature differences (within 20 m of the surface and bottom), or T_{cp} , to determine the strength of the stratification. This is done for the XBT section before each ring passes (Figure 10, left column), for the XBT section during the ring passage that ΔT_s can be calculated (Figure 10, right column), and the XBT section after the

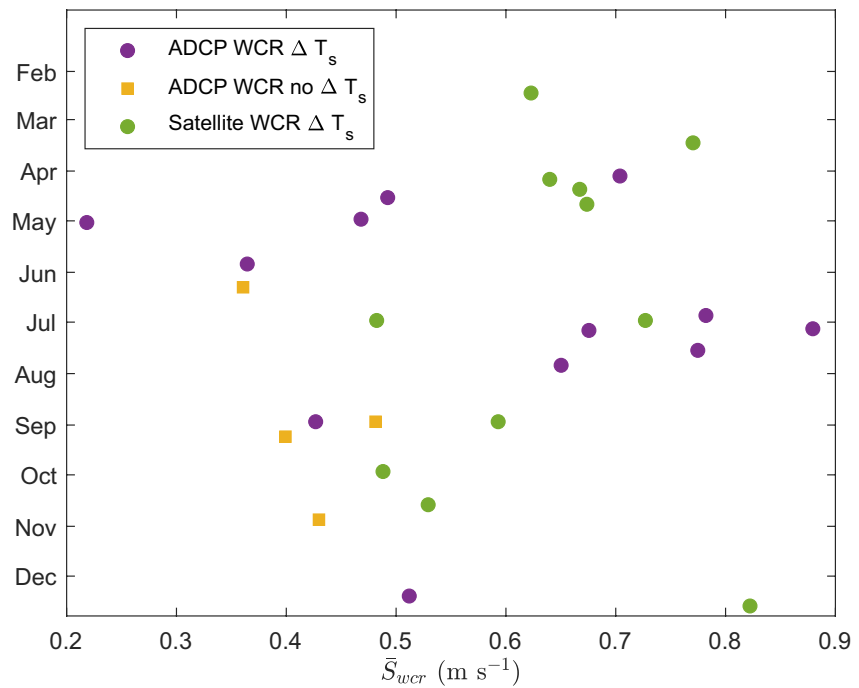


Figure 9. The speed of the rings (\bar{S}_{wcr}) and the mean day of the year the ring was on the Oleander Line. Purple dots are when ΔT_s is calculated, yellow squares do not have expendable bathythermographs (XBT) data before and after the ring passes, green dots are rings with XBT data that were identified through satellite tracking.

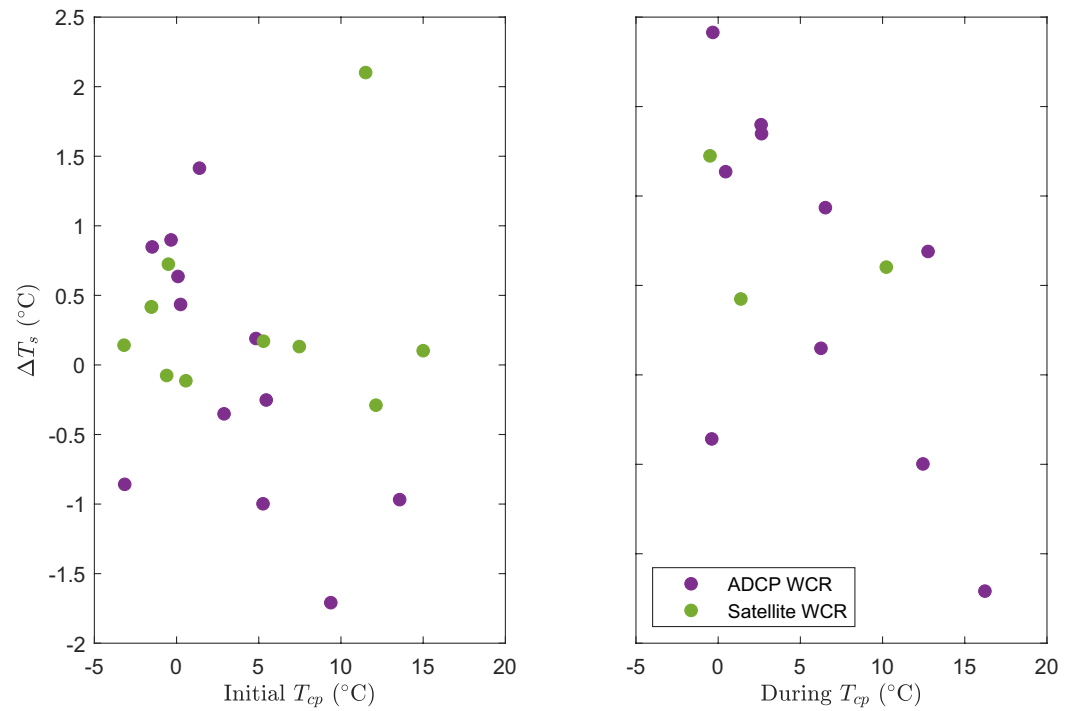


Figure 10. ΔT_s plotted against the temperature stratification (T_{cp}) in the expendable bathythermograph (XBT) section before the ring passes (left) and the XBT section when the ring is intersecting the Oleander track (right). There are only 10 XBT sections during the ring when T_{cp} can also be calculated. ΔT_s is correlated with both the T_{cp} before the ring passes ($r = -0.6$ and $p < 0.05$) and T_{cp} when the ring is on the Oleander Line ($r = -0.66$ and $p < 0.05$).

ring has passed (not shown). T_{cp} before a ring passes and T_{cp} during the ring passing are both significantly correlated to ΔT_s at the 95% confidence level, while T_{cp} after the ring has passed is not correlated with ΔT_s ($r = -0.50$ and $p = 0.09$). Additionally, we find that δT_{wcr} is significantly correlated to T_{cp} before ($r = 0.85$, $p < 0.01$) and during a ring ($r = 0.79$ and $p < 0.01$) at the 95% confidence level. This suggests that stronger stratification limits the ability of a ring to warm the shelf and can act as a barrier for ring water to intrude onto the shelf.

To understand how stratification limits the ability for ring water to warm the shelf, we estimate the density of the ring water. Using data from the TSG, we find that the surface salinity of WCRs ranges from 35 to 36, while surface temperatures range from 20°C to 28°C, mostly varying with season. Taking the average of these values, we can estimate that the density of the ring water near the surface as $\rho = 1024 \text{ kg m}^{-3}$. Shelf water has salinity values from 32 to 34. Given a salinity of 33, the ring water has equal density to the shelf water when the shelf is at a temperature of 17°C. Using climatological temperature sections from the Oleander XBTs, during June–September, the ring water would be more dense than the shelf surface water and less dense than the Cold Pool water. For this density structure, ring water would have to intrude onto the shelf as a mid-depth salinity maximum intrusion. Our estimates here are consistent with past research which only found mid-depth salinity intrusions during the summer and fall months (Churchill et al., 1986). It is likely that mid-depth intrusions have a limited ability to warm the shelf. Linear models have shown that enhanced vertical stratification, which occurs in the summer months, limits the ability for cross-shelf motions across the slope, which would reduce the warming impact of rings (Chapman & Brink, 1987). Past rings which have been studied and drastically warmed the shelf have been primarily concentrated at the surface or bottom (Chen et al., 2014; Gawarkiewicz et al., 2019). This aids in explaining why shelf temperatures do not warm when the Cold Pool is present, but does not explain why there is cooling after some rings have passed.

One possible mechanism for the observed cooling could be upwelling of colder waters due to the divergence driven by the trailing edge of the ring. The divergence of the rings with ADCP data was calculated in Section 3.1 based on the last available velocity section during each WCR. We plot w_{up} versus ΔT_s (Figure 11). There is no correlation between w_{up} as a ring passes and ΔT_s ($r = -0.43$ and $p < 0.20$). However, if we remove the most positive ΔT_s , there is a strong linear relationship between w_{up} and ΔT_s ($r = -0.8$ and $p < 0.01$). The strong relationship upon removing a singular ring suggests that for some rings, upwelling may be an important mechanism to explain the changes to shelf temperatures from a ring. However, there are other processes (e.g., storms) which impact shelf temperature anomalies over the timespan that it takes for rings to transit past the shelf. Because of the complicated nature of the shelfbreak system, as well as the variability between WCRs, it is important to further study upwelling due to rings, as well as how this may impact the shelf.

4. Conclusion

WCRs impact the shelf system by both modifying the velocity fields when the ring is abutting the shelf, and by creating lasting temperature changes. The velocity on the shelf is most affected by rings that have high velocities and are closer to the shelf. We confirm past findings from studies south of Martha's Vineyard that the Shelfbreak Jet is accelerated as a ring approaches, likely due to the steepening of the Shelfbreak Front, while at the trailing edge of the ring the Shelfbreak Jet tends to be slower (Gawarkiewicz et al., 2001; Pickart et al., 1999). There is also a divergence in the cross-shelf velocities at the trailing edge of the rings, leading to the possibility of enhanced upwelling.

The shelf temperature's relationship with rings is more complicated, with multiple factors likely influencing how the temperatures change on the shelf due to a ring. There is a strong seasonality in the rings' ability to impact shelf temperature. Stronger stratification on the shelf is connected to rings that had a net cooling impact on the shelf temperature. The stratification likely limits the ability for ring water to move onto the shelf as the surface density of ring water requires it to intrude sub-surface. Sub-surface intrusions of ring/slope water have only been found during the summer months due to the density structure on the shelf (Aikman, 1984; Churchill et al., 1986). We note that past observations of rings which warmed the shelf took place before the seasonal summer stratification was set up, consistent with our observations (Gawarkiewicz et al., 2019; Zhang & Gawarkiewicz, 2015).

In addition, rings associated with stronger upwelling due to the divergence in cross-shelf velocities, are correlated with shelf cooling, while weak upwelling corresponds with shelf warming. Enhanced upwelling has large consequences for the impact that the ring has not just on temperature, but on the productivity of the shelf. Past studies

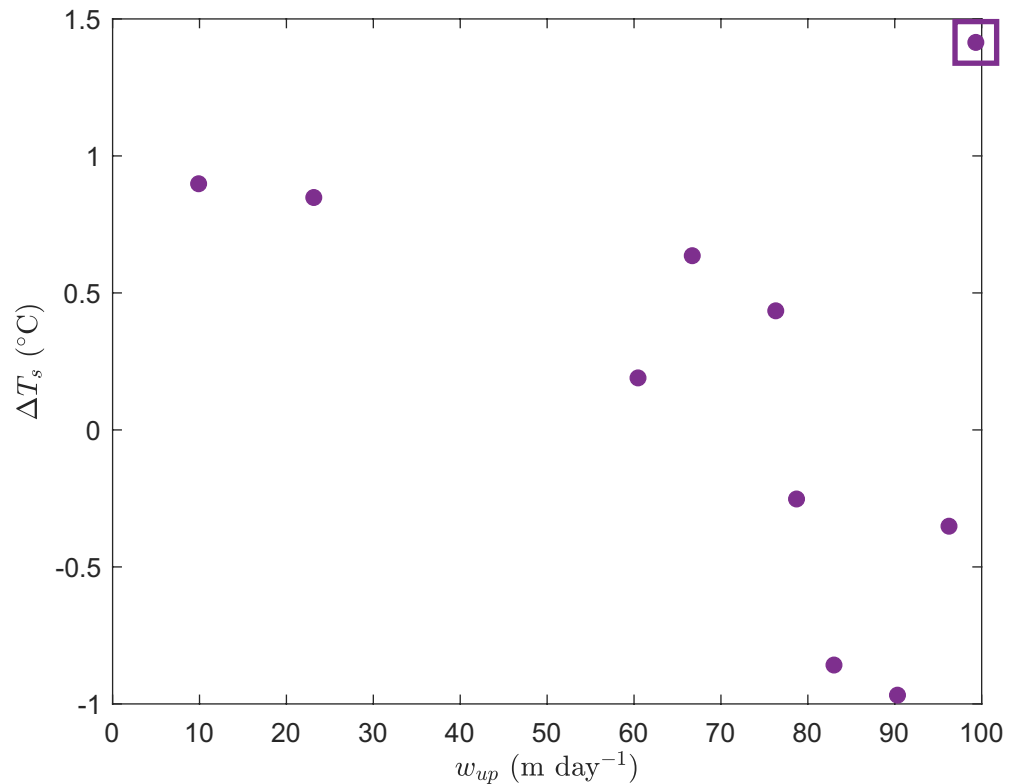


Figure 11. ΔT_s plotted against the upwelling velocities (w_{up}) estimated from Equation 1. This relationship is not significant at the 95% confidence interval for all data ($r = -0.43$ and $p < 0.20$), but with removal of the largest ΔT_s is significant (data point removed outlined with square, $r = -0.8$ and $p < 0.01$). 10 rings had both expendable bathythermograph data as well as reliable acoustic Doppler current profiler data to calculate upwelling on the trailing edge of the ring.

near Georges Bank found enhanced chlorophyll after a ring had passed the region (J. Ryan et al., 2001). This was attributed to upwelling on the trailing edge of the ring as divergent cross-shelf velocities were observed. We were not able to find any significant changes to the surface chlorophyll on the shelf, but instead noticed advection of chlorophyll off the shelf due to the ring. Thus, the timing of rings relative to seasonal blooms could have significant impacts on the shelf/slope productivity, while further study is needed to understand if enhanced upwelling from rings modifies chlorophyll levels within this region.

We have established that ring properties vary greatly from one ring to the next, and thus to understand the overall impact that rings have on the shelf, it is necessary to study multiple rings. Because the CMV *Oleander* is consistently monitoring the same line, the data are incredibly valuable for studying many individual events of rings impinging on the shelf. However, these data are limited to a two dimensional framework, and thus developing a dynamical understanding for the differences between rings is limited. We have noted key properties of rings that deserve greater study through modeling or long-term monitoring data sets with observations in three dimensions.

Data Availability Statement

ADCP data product is available at <https://doi.org/10.5281/zenodo.3935983>, XBT data product is available at <https://doi.org/10.5281/zenodo.3967332>, raw CMV *Oleander* data are available at <http://oleander.bios.edu/data/>, altimetry data are available at <https://marine.copernicus.eu/>, sea surface temperature data are available at from the NCDC website (<https://www.ncdc.noaa.gov/oisst>), and chlorophyll-a data are available from NASA ocean color website (<https://oceancolor.gsfc.nasa.gov/data/seawifs/>).

Acknowledgments

J. Forsyth and M. Andres were supported by OCE-1924041. J. Forsyth and G. Gawarkiewicz were supported by ONR N00014-19-1-2646. G. Gawarkiewicz was also supported by NSF under grant OCE-1851261.

References

Aikman, F., III. (1984). Pycnocline development and its consequences in the Middle Atlantic Bight. *Journal of Geophysical Research*, 89(C1), 685–694. <https://doi.org/10.1029/jc089ic01p00685>

Barth, J. A., Bogucki, D., Pierce, S. D., & Kosro, P. M. (1998). Secondary circulation associated with a Shelfbreak front. *Geophysical Research Letters*, 25(15), 2761–2764. <https://doi.org/10.1029/98gl02104>

Beardsley, R. C., Chapman, D. C., Brink, K. H., Ramp, S. R., & Schlitz, R. (1985). The nantucket shoals flux experiment (NSFE79). Part I: A basic Description of the current and temperature variability. *Journal of Physical Oceanography*, 15(6), 713–748. [https://doi.org/10.1175/1520-0485\(1985\)015<0713:tmsfep>2.0.co;2](https://doi.org/10.1175/1520-0485(1985)015<0713:tmsfep>2.0.co;2)

Bisagni, J. J. (1983). Lagrangian current measurements within the Eastern Margin of a Warm-Core Gulf Stream Ring. *Journal of Physical Oceanography*, 13(4), 709–715. [https://doi.org/10.1175/1520-0485\(1983\)013<0709:lcmwte>2.0.co;2](https://doi.org/10.1175/1520-0485(1983)013<0709:lcmwte>2.0.co;2)

Cenedese, C., Todd, R. E., Gawarkiewicz, G. G., Owens, W. B., & Shcherbina, A. Y. (2013). Offshore transport of shelf waters through interaction of vortices with a Shelfbreak current. *Journal of Physical Oceanography*, 43(5), 905–9191. <https://doi.org/10.1175/jpo-d-12-0150.110.1175/JPO-D-12-0150.1>

Chapman, D. C., & Brink, K. H. (1987). Shelf and slope circulation induced by fluctuating offshore forcing. *Journal of Geophysical Research*, 92(C11), 11741–11759. <https://doi.org/10.1029/jc092ic11p11741>

Chelton, D. B., Schlax, M. G., & Samelson, R. M. (2011). Global observations of nonlinear mesoscale eddies. *Progress in Oceanography*, 91(2), 167–216. <https://doi.org/10.1016/j.pocean.2011.01.002>

Chen, K., He, R., Powell, B. S., Gawarkiewicz, G., Moore, A. M., & Arango, H. G. (2014). Data assimilative modeling investigation of Gulf Stream Warm Core Ring interaction with continental shelf and slope circulation. *Journal of Geophysical Research: Oceans*, 119(9), 5968–5991. <https://doi.org/10.1002/2014JC00989810.1002/2014JC009898>

Churchill, J. H., Cornillon, P. C., & Milkowski, G. W. (1986). A cyclonic eddy and shelf-slope water exchange associated with a gulf stream warm-core ring. *Journal of Geophysical Research: Oceans*, 91(C8), 9615–9623. <https://doi.org/10.1029/jc091ic08p09615>

Flagg, C. N., Schwartz, G., Gottlieb, E., & Rossby, T. (1998). Operating an acoustic Doppler current profiler aboard a container vessel. *Journal of Atmospheric and Oceanic Technology*, 15, 257–271. [https://doi.org/10.1175/1520-0426\(1998\)015<0257:oadcp>2.0.co;2](https://doi.org/10.1175/1520-0426(1998)015<0257:oadcp>2.0.co;2)

Forsyth, J., Andres, M., & Gawarkiewicz, G. (2015). Recent accelerated warming of the continental shelf off New Jersey: Observations from the CMV Oleander expendable bathythermograph line. *Journal of Geophysical Research: Oceans*, 120(3), 2370–2384. <https://doi.org/10.1002/2014JC010516>

Forsyth, J., Andres, M., & Gawarkiewicz, G. (2020). Shelfbreak jet structure and variability off New Jersey using ship of opportunity data from the CMV oleander. *Journal of Geophysical Research: Oceans*, 125(9), e2020JC016455. <https://doi.org/10.1029/2020jc016455>

Gangopadhyay, A., Gawarkiewicz, G., Silva, E. N. S., Monim, M., & Clark, J. (2019). An observed regime shift in the formation of Warm Core Rings from the Gulf Stream. *Scientific Reports*, 9(12319). <https://doi.org/10.1038/s41598-019-48661-9>

Gangopadhyay, A., Gawarkiewicz, G., Silva, E. N. S., Silver, A. M., Monim, M., & Clark, J. (2020). A census of the Warm-Core Rings of the Gulf Stream: 1980–2017. *Journal of Geophysical Research: Oceans*, 125(8), e2019JC016033. <https://doi.org/10.1029/2019jc016033>

Gawarkiewicz, G., Bahr, F., Beardsley, R. C., & Brink, K. H. (2001). Interaction of a slope eddy with the Shelfbreak front in the Middle Atlantic Bight. *Journal of Physical Oceanography*, 31, 2783–2796. [https://doi.org/10.1175/1520-0485\(2001\)031<2783:ioasew>2.0.co;2](https://doi.org/10.1175/1520-0485(2001)031<2783:ioasew>2.0.co;2)

Gawarkiewicz, G., Chen, K., Forsyth, J., Bahr, F., Mercer, A. M., Ellertson, A., et al. (2019). Characteristics of an advective marine heatwave in the Middle Atlantic Bight in early 2017. *Frontiers in Marine Science*, 6, 712. <https://doi.org/10.3389/fmars.2019.00712>

Griffin, R. B. (1999). Sperm whale distributions and community ecology associated with a warm-core ring off Georges Bank. *Marine Mammal Science*, 15(1), 33–51. <https://doi.org/10.1111/j.1748-7692.1999.tb00780.x>

Houghton, R. W., & Visbeck, M. (1998). Upwelling and convergence in the Middle Atlantic Bight Shelfbreak front. *Geophysical Research Letters*, 25(15), 2765–2768. <https://doi.org/10.1029/98gl02105>

Joyce, T. (1984). Velocity and hydrographic structure of a gulf stream warm-core ring. *Journal of Physical Oceanography*, 14(5), 936–947. [https://doi.org/10.1175/1520-0485\(1984\)014<0936:vahsoa>2.0.co;2](https://doi.org/10.1175/1520-0485(1984)014<0936:vahsoa>2.0.co;2)

Joyce, T., Bishop, J. K., & Brown, O. B. (1992). Observations of offshore shelf-water transport induced by a warm-core ring. *Deep-Sea Research Part A. Oceanographic Research Papers*, 39, S97–S113. [https://doi.org/10.1016/s0198-0149\(11\)80007-5](https://doi.org/10.1016/s0198-0149(11)80007-5)

Lentz, S. J. (2008). Observations and a model of the mean circulation over the Middle Atlantic Bight continental shelf. *Journal of Physical Oceanography*, 38(6), 1203–1221. <https://doi.org/10.1175/2007JPO3768.110.1175/2007JPO3768.1>

Morgan, C. W., & Bishop, J. M. (1977). An example of gulf stream eddy-induced water exchange in the Mid-Atlantic Bight. *Journal of Physical Oceanography*, 7, 472–479. [https://doi.org/10.1175/1520-0485\(1977\)007<0472:aeogse>2.0.co;2](https://doi.org/10.1175/1520-0485(1977)007<0472:aeogse>2.0.co;2)

Ning, J., Chen, K., & Gaube, P. (2021). Diverse variability of surface chlorophyll during the evolution of Gulf Stream Rings. *Geophysical Research Letters*, 48(5), e2020GL091461. <https://doi.org/10.1029/2020gl091461>

Oliver, H., Zhang, W. G., Smith, W. O., Jr, Alatalo, P., Chappell, P. D., Hirzel, A. J., & McGillicuddy, D. J., Jr. (2021). Diatom hotspots driven by western boundary current instability. *Geophysical Research Letters*, 48(11), e2020GL091943. <https://doi.org/10.1029/2020gl091943>

Pickart, R. S., Torres, D. J., McKee, T. K., Caruso, M. J., & Przystup, J. E. (1999). Diagnosing a meander of the shelf break current in the Middle Atlantic Bight. *Journal of Geophysical Research: Oceans*, 104(C2), 3121–3132. <https://doi.org/10.1029/1998jc900066>

Reynolds, R. W., Smith, T. M., Liu, C., Chelton, D. B., Casey, K. S., & Schlax, M. G. (2007). Daily high-resolution-blended analyses for sea surface temperature. *Journal of Climate*, 20(22), 5473–5496. <https://doi.org/10.1175/2007JCL11824.110.1175/2007JCL11824.1>

Ryan, J., Yoder, J., & Townsend, D. (2001). Influence of a gulf stream warm-core ring on water mass and chlorophyll distributions along the southern flank of Georges bank. *Deep Sea Research Part II: Topical Studies in Oceanography*, 48(1), 159–178. [https://doi.org/10.1016/S0967-0645\(00\)00117-X](https://doi.org/10.1016/S0967-0645(00)00117-X)

Ryan, J. P., Yoder, J. A., Barth, J. A., & Cornillon, P. C. (1999). Chlorophyll enhancement and mixing associated with meanders of the shelf break front in the Mid-Atlantic bight. *Journal of Geophysical Research*, 104(C10), 23479–23493. <https://doi.org/10.1029/1999jc900174>

Wei, J., Wang, D.-P., & Flagg, C. N. (2008). Mapping gulf stream warm core rings from shipboard adcp transects of the oleander project. *Journal of Geophysical Research*, 113(C10). <https://doi.org/10.1029/2007JC004694>

Worst, J. S., Donohue, K. A., & Rossby, T. (2014). A comparison of vessel-mounted acoustic Doppler current profiler and satellite altimeter estimates of sea surface height and transports between New Jersey and Bermuda along the CMV Oleander route. *Journal of Atmospheric and Oceanic Technology*, 31(6), 1422–1433. <https://doi.org/10.1175/jtech-d-13-00122.110.1175/JTECH-D-13-00122.1>

Zhang, W. G., & Gawarkiewicz, G. (2015). Dynamics of the direct intrusion of Gulf Stream Ring water onto the Mid-Atlantic Bight Shelf. *Geophysical Research Letters*, 42(18), 7687–7695. <https://doi.org/10.1002/2015gl065530>